FULL PAPER

Over 1.1 eV Workfunction Tuning of Cesium Intercalated Metal Oxides for Functioning as Both Electron and Hole Transport Layers in Organic Optoelectronic Devices

*Xinchen Li, Fengxian Xie, Shaoqing Zhang, Jianhui Hou, and Wallace C. H. Choy**

In this paper, over 1.1 eV continuous tuning of metal oxides workfunction is realized by cesium intercalation, making the metal oxide function as both electron transport layer and hole transport layer in organic optoelectronic devices. The demonstrated metal oxides are commonly used molybdenum oxide and vanadium oxide. The proposed approach of synthesizing cesium intercalated metal oxides has interesting properties of room-temperature, ambient atmosphere, water free and solution process, favoring the formation of metal oxides as carrier transport layers at different regions in multi-layered devices and large scale fabrication of organic optoelectronics at low cost. Besides the wide range of controllable workfunction adjustment, band structures, and electrical properties are investigated in detail, to understand the effects of cesium intercalation on metal oxides. The device results show that, using the proposed cesium intercalation approach, each of the two investigated metal oxides can function as both ETL and HTL in organic solar cells and organic light emitting diodes with very good device performances. Consequently, with the interesting properties in film synthesis, the proposed cesium intercalated metal oxides can achieve continuously workfunction tuning over a large range and contribute to evolution of the simple route for fabricating high performance organic optoelectronic devices.

1. Introduction

Over the past decades, organic solar cells (OSCs) and organic light emitting diodes (OLEDs) have shown great potential in addressing green energy applications and reducing fabrication costs.[1–3] One of the most promising advantages of OSCs and OLEDs is the potential to realize all solution, room-temperature and cost-effective processing method, which can greatly simplify device fabrication, lower production costs, and improve the availability to the general public.

X. Li, F. Xie, Prof. W. C. H. Choy
Department of Electrical and Electronic Engineering
The University of Hong Kong
Pokfulam Road, Hong Kong, China
E-mail: chchoy@eee.hku.hk
S. Zhang, Prof. J. Hou
Institute of Chemistry
Chinese Academy of Sciences
Beijing 100190, China

DOI: 10.1002/adfm.201401969

Up to now, most of the interfacial layer materials of OSCs and OLEDs are generally formed by thermal evaporation method or solution process with high temperature annealing treatment. For example, thermally evaporated MoO_3 as hole transport layer (HTL) and Ca as electron transport layer (ETL) typically require high vacuum condition for deposit and thus high power consumption for the process.[4] Although OSCs can reach high power conversion efficiency (PCE), solution processed MoO_3 or TiO_2 using precursor methods for forming carrier transport layers usually need high temperature annealing process of the films on substrates.[5] It is a concern that, thermal evaporation methods or high temperature annealing processes may cause the molecular scission for polymers and modifications in crystallization of the blend active layer, which will deteriorate the performance of OSCs or OLEDs and limit the structure of the device.[6] Moreover, the high energy consumption and uneconomical cost of these processes act inconsistent with the idea of the green energy applications. Consequently, it is of great importance to develop the high performance carrier transport layers featuring in the room-temperature and solution-processed approach.

Efficient charge transport can be realized when the Fermi level of metal oxide substrate approach to the ionization energy of organic material.[7] Molybdenum oxide (MoO_3) and vanadium oxide (V_2O_5) with the high workfunction properties have been the most promising metal oxides working as HTLs in OSCs and OLEDs.[3,8–10] Typically, the layered crystal structure of MoO_3 and V_2O_5 are held by the presence of van der Waals forces,[11] which can allow intercalating other atom or metal cation into the metal oxides. Early studies have shown that electrical properties and electrochemical performance of MoO_3 or V_2O_5 could be improved by the introduction of other cations such as H, Ti, K, Al, Mn, Cu, and Sn.[12] Besides, previous reports have shown that Cs_2CO_3 can be formed as ETL by solution process with high temperature annealing or evaporation methods in OSCs and OLEDs due to the low workfunction of the composite film.[9,13] There are also reports showing that the Cs_2CO_3 mixed with TiO_2 at a 1:1 weight ratio can further

improve the performance of TiO_2 ETL in organic optoelectronic devices.[14] These metal oxides based carrier transport layers usually need high annealing temperature process or co-evaporation methods.

In this paper, we propose and demonstrate a large and continuous workfunction tuning of over 1.1 eV in MoO_3 and V_2O_5 by the approach of cesium intercalation with a wide mole ratio of Cs:Mo and Cs:V from 0:1 (pristine metal oxides) to 0.75:1 (Cs intercalated metal oxides). The synthesis approach has the interesting features of room temperature, room atmosphere, water free and solution process. With the large adjustment and controllable workfunction modification, the band structures and electrical properties favor each of the two metal oxides functioning as both ETL and HTL within one organic optoelectronic device. We demonstrate that ETL and HTL made from the same based metal oxide by this unified approach can yield efficient performance comparable to traditional non-metal oxide organic optoelectronic devices including OSCs and OLEDs. This unified Cs intercalation approach achieves large workfunction tuning of metal oxides and offers a simple route to fabricate high performance organic optoelectronic devices.

2. Results and Discussion

2.1. A Wide Tuning of Electrical Properties of Cesium Intercalated MoO_3 and V_2O_5

Various mole ratio of cesium intercalated MoO_3 (Cs_xMoO_3) and V_2O_5 ($Cs_xV_2O_5$) are formed from corresponding cesium metal (Mo or V) bronze solutions. The bronze solutions are synthesized from molybdenum powder or vanadium powder which dissolved in ethanol and hydrogen peroxide mixed solution with incorporated cesium element at different calculated mole ratio. The final solution is diluted with ethanol to have an optimized Cs intercalated metal oxides thickness after spin-coating as described in detail in experimental section. The synthesis scheme with products of each step as additional description is described in Supporting Information. The element components of different synthesized metal oxides are measured by energy-dispersive X-ray spectroscopy (EDX) as shown in Figure S1 and Table S1 in Supporting Information. The EDX results of Cs intercalated metal oxides show clear Cs major peaks and reveal that the metal oxides synthesized from our method are free from impurities. Notably, compared to pristine MoO_3 and V_2O_5, Cs_xMoO_3 and $Cs_xV_2O_5$ can approach large workfunction tuning with different electrical properties as described below.

The energy level alignment of the metal oxides with adjacent layers has a great influence in organic optoelectronic devices performance.[7,15] Here, we use the Kelvin-Probe measurement to investigate the workfunction variation of the metal oxides by Cs intercalating process and the results are shown in **Table 1**. It is found that the pristine MoO_3 on the indium tin oxide (ITO) substrate exhibits a workfunction of 5.32 eV while the workfunction of pristine V_2O_5 is 5.41 eV. The high workfunction of MoO_3 and V_2O_5 can be aligned well with the highest occupied molecular orbital (HOMO) of typical polymer donors. When the concentration of intercalated Cs increases, the workfunction of Cs_xMoO_3 and $Cs_xV_2O_5$ can be tuned continuously from 5.32 eV to 4.17 eV (i.e., the change of workfunction is over 1.15 eV) and from 5.41 eV to 4.12 eV (i.e., the change of workfunction is over 1.29 eV), respectively. Using typical bulk heterojunction OSCs as an example, the commonly used acceptor materials [6,6]-phenyl C_{61}-butyric acid methyl ester ($PC_{61}BM$) and [6,6]-phenyl C_{71}-butyric acid methyl ester ($PC_{71}BM$) have the lowest unoccupied molecular orbital (LUMO) around 4 eV. With appropriate amount of Cs, the workfunction of the metal oxides can align well with LUMO of the organic acceptor. Indeed, the Cs intercalated metal oxides with 0.5:1 mole ratio gives the best performance in organic optoelectronic devices as described in next section. The morphology and local surface potential of the metal oxide films are also investigated by Kelvin probe force microscope (KPFM). The films of different metal oxides were formed by spin-coating prepared solutions at 3000 rpm on the ITO/glass substrates. **Figure 1** shows the KPFM image results of MoO_3, $Cs_{0.5}MoO_3$, V_2O_5 and CsV_2O_5. The root-mean-square (RMS) roughness of MoO_3, $Cs_{0.5}MoO_3$, V_2O_5 and CsV_2O_5 are 2.16 nm, 2.10 nm, 2.64 nm and 3.34 nm respectively. The small RMS roughness indicates that metal oxides films can form compactly as buffer layers on the electrode and reduce the leakage current. As shown in Figure 1e to h, the smooth surface potential of metal oxides reveal that Cs intercalated metal oxides with good film quality are formed.

Table 1. The workfunction variation of Cs_xMoO_3 and $Cs_xV_2O_5$ with different Cs ratio. The energy-level offset of Cs intercalated metal oxides from the pristine metal oxides is defined as ΔE_F.

Mole ratio of Cs : Mo or V	Cs_xMoO_3		$Cs_xV_2O_5$	
	Workfunction [eV]	ΔE_F [eV]	Workfunction [eV]	ΔE_F [eV]
0 : 1	5.32	0	5.41	0
0.07 : 1	5.03	0.29	5.15	0.26
0.12 : 1	4.84	0.48	4.91	0.50
0.25 : 1	4.53	0.79	4.57	0.84
0.5 : 1	4.28	1.04	4.19	1.22
0.75 : 1	4.17	1.15	4.12	1.29

To further understand the mechanism of workfunction tuning of metal oxides by Cs intercalation, electrical properties and band structures of MoO_3, $Cs_{0.5}MoO_3$, V_2O_5 and CsV_2O_5 formed on ITO substrates have been studied by using ultraviolet photoelectron spectroscopy (UPS). **Figure 2**a shows that when Cs:Mo ratio increases from 0:1 to 0.5:1, the secondary-electron cut-off shifts 1.11 eV and Fermi edge shifts 0.23 eV. Meanwhile, when Cs:V ratio increases from 0:1 to 0.5:1, the secondary-electron cut-off and Fermi edge shift 1.28 eV and 0.56 eV respectively as shown in Figure 2b. The clear shifts of the UPS results indicate that the energy band structures of MoO_3 and V_2O_5 films are changed simultaneously with the Cs intercalating process. In the meantime, the optical band gap (E_{opt}), which was measured by ellipsometry, are shown in Figure 2c,d. Interestingly, the E_{opt} of MoO_3 enlarges from 2.97 eV to 3.26 eV when the Cs:Mo ratio changes from 0:1 to 0.5:1. For the case of V_2O_5, E_{opt} increases from 3.23 eV to 3.31 eV. The E_{opt} widening of the Cs intercalated metal oxides reveals that higher energy excitation is required for electron transitions from the valence band to the conduction band, which also occur

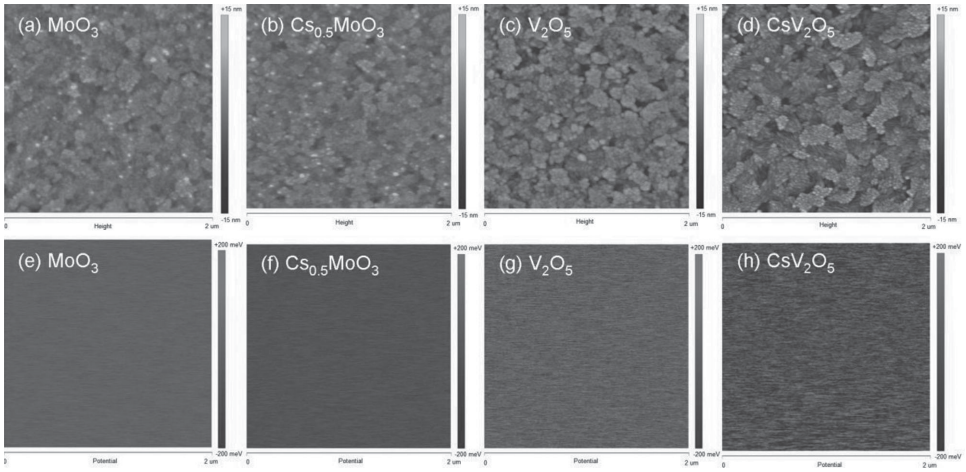

Figure 1. KPFM results of different metal oxides with measured area of 2 μm × 2 μm, including a–d) surface height image of MoO_3, $Cs_{0.5}MoO_3$, V_2O_5, CsV_2O_5 (the scale bar is ±15 nm), e–h) surface potential of metal oxides (the scale bar is ±200 meV).

in heavily doped n-type semiconductor and can be explained by band-filling effect.[16] As a consequence, the enlarged band gap by Cs intercalation makes the metal oxides become effective electron transport layers with good hole blocking properties.

From the results of UPS and E_{opt}, the energy band structure diagrams of pristine MoO_3, V_2O_5 and Cs_xMoO_3, $Cs_xV_2O_5$ are obtained as shown in Figure 2e,f. The Fermi level of MoO_3 can be significantly modified from 5.35 eV to 4.24 eV and that of V_2O_5 from 5.43 eV to 4.15 eV by Cs intercalation. The work-function of semiconductor is highly depended on the Fermi level of the band structure. The Fermi levels of intercalated metal oxides which were determined in relevant energy band structures which re-confirm the Kelvin-Probe results as shown in Table 1. Importantly, from detail energy band structures, it is clearly observed that Cs_xMoO_3 and $Cs_xV_2O_5$ become more n-type semiconductor (i.e., Fermi levels approach more to conduction bands), which offers better electron transport properties for applications in organic optoelectronic devices.

2.2. Performance of Organic Optoelectronic Devices

2.2.1. OSCs with Cs Intercalated Metal Oxides as both ETL and HTL

The OSCs have the structure of ITO/pristine metal oxide/polymer blend active layer/Cs intercalated metal oxide/Al as shown in **Figure 3**a. The active layer is low band gap donor of poly[(((2-hexyldecyl)sulfonyl)-4,6-di(thiophen-2-yl)thieno[3,4-b]thiophene-2,6-diyl)-alt-(4,8-bis((2-ethylhexyl)oxy)benzo[1,2-b:4,5-b']dithiophene-2,6-diyl)] (PBDTDTTT-S-T)[17] blended with acceptor of [6,6]-phenyl C_{71}-butyric acid methyl ester ($PC_{71}BM$). In the OSCs, the HTL and ETL are either MoO_3 and $Cs_{0.5}MoO_3$ or V_2O_5 and CsV_2O_5 respectively. The thickness of the $Cs_{0.5}MoO_3$ and CsV_2O_5 are optimized as shown in Table S2 and Figure S2 in Supporting Information. Details of device fabrication are described in experimental section.

By using Cs intercalated MoO_3 and V_2O_5 and pristine metal oxides as both of ETL and HTL, the performances of optimized OSCs are summarized in **Table 2**. By using the MoO_3 and $Cs_{0.5}MoO_3$ as HTL and ETL respectively, the optimized OSC has short-circuit current density (J_{SC}) of 16.08 mA cm^{-2}, an open-circuit voltage (V_{OC}) of 0.68 V, a fill factor (FF) of 66.94% and a PCE of 7.32%. Meanwhile, by using CsV_2O_5 as ETL and V_2O_5 as HTL, the optimized OSC has J_{SC} of 16.38 mA cm^{-2}, V_{OC} of 0.68 V, FF of 67.23%, and PCE of 7.49%. The performances are comparable to the reported OSCs with the normal structure of ITO/PEDOT:PSS/PBDTDTTT-S-T:$PC_{71}BM$/Ca/Al which gives average PCE of 7.48%.[13] The incident photon-to-current conversion efficiency (IPCE) spectra of different OSCs are given in Figure S3 in Supporting Information. The performance of OSCs using metal oxide as HTL and a bare layer Al as cathode is shown in Figure S4 and Table S3 in Supporting Information.

Regarding the Cs intercalation effects on OSCs, the device performances of OSCs using metal oxides with different Cs mole ratio as electron transport layer are shown in **Figure 4**a,b as well as **Table 3**. It can be observed that the performance of OSCs gradually improved when the Cs content increases. The optimal performance can be achieved when the Cs:Mo and Cs:V mole ratios reach 0.5:1. By using larger Cs ratio of the metal oxides films, the performance of OSC slightly decreases especially for the J_{SC} and FF. This may be due to an excess of Cs cations intercalated into MoO_3 and V_2O_5 layered structure which causes defects and the carrier transport properties degradation.[18] Moreover, inverted OSCs using metal oxides and Cs intercalated metal oxides as HTLs and ETLs can also be realized. The OSC with the structures of ITO/$Cs_{0.5}MoO_3$/PBDTDTTT-S-T:$PC_{71}BM$/MoO_3/Ag gives J_{SC} of 15.63 mA cm^{-2}, V_{OC} of 0.61 V, FF of 62.85% and PCE of 6.00%, and OSC of ITO/CsV_2O_5/PBDTDTTT-S-T:$PC_{71}BM$/V_2O_5/Ag gives J_{SC} of 15.79 mA cm^{-2}, V_{OC} of 0.63 V, FF of 61.10%, and PCE of 6.08%. The details of the organic optoelectronic devices with inverted structure will be discussed and reported in elsewhere.

In OSCs, an optimal V_{OC} can be generally realized by forming Ohmic contacts between the electrodes and the polymer blend active layer. Otherwise, V_{OC} will reduce when there are Schottky

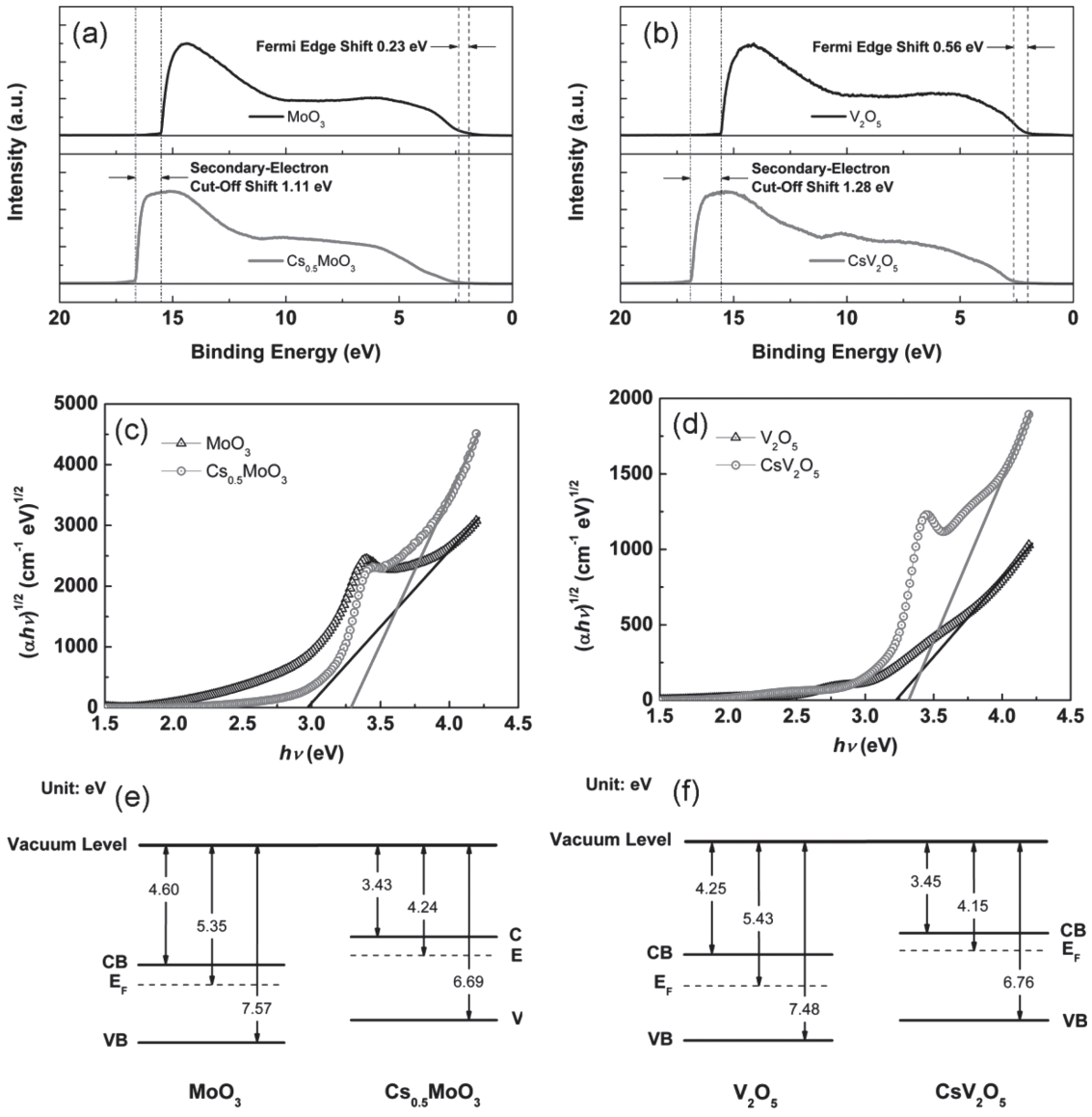

Figure 2. a,b) UPS results of MoO_3, $Cs_{0.5}MoO_3$, V_2O_5 and CsV_2O_5. c,d) Optical band gap (E_{opt}) results from the plot of $(\alpha h\nu)^{1/2}$ verse photon energy ($h\nu$) of MoO_3, $Cs_{0.5}MoO_3$, V_2O_5 and CsV_2O_5. E_{opt} can be taken from the intersection of extrapolated line with the energy axis. Different E_{opt} of MoO_3, $Cs_{0.5}MoO_3$, V_2O_5, and CsV_2O_5 are 2.97 eV, 3.26 eV, 3.23 eV, and 3.31 eV respectively. e,f) Detailed energy band structures calculated from the UPS and E_{opt} results of different metal oxides.

contacts at the interfaces. Here, the energy-level offset between the HTL and ETL is defined as ΔE_F. By change the Cs content in metal oxides, the variation of workfunction (see **Figure 5**a) and V_{OC} dependent on ΔE_F (see Figure 5b) are investigated. At low Cs content such as Cs:Mo and Cs:V less than 0.25:1, a general increase of V_{OC} is accompanied by the increase of ΔE_F, which illustrates that the potential barrier of non-Ohmic contacts between the ETL and the active layer is the cause of the carrier energy loss, and thus V_{OC} degradation.[1,19] With further increase of the Cs ration exceeding 0.5:1, V_{OC} remains around the value of 0.68 V and gives an optimal device performance. It should be noted that, V_{OC} and the corresponding $(1/q)\Delta E_F$ have an electrical potential difference of about 0.3 V, which well agrees with the previous theoretical and experimental reports of a surplus potential difference of 0.3 eV for efficient charge dissociation.[20] Importantly, by adjusting the Cs content in MoO_3 and V_2O_5, the energy-level offset of the carrier transport layers can be tuned to achieve an optimal V_{OC} by using effective ETL and HTL with the expression:

$$\Delta E_F \geq qV_{OC} + 0.3 \text{ eV} \quad (1)$$

where q is the electron charge.

The efficiency of OSCs also strongly depends on the J_{SC} and FF. By changing the Cs content in metal oxides, the barrier between the ETL and the polymer blend active layer will change, which significantly influences J_{SC} and FF and thus PCE of the OSCs as shown in Figure 5c,d. Previously

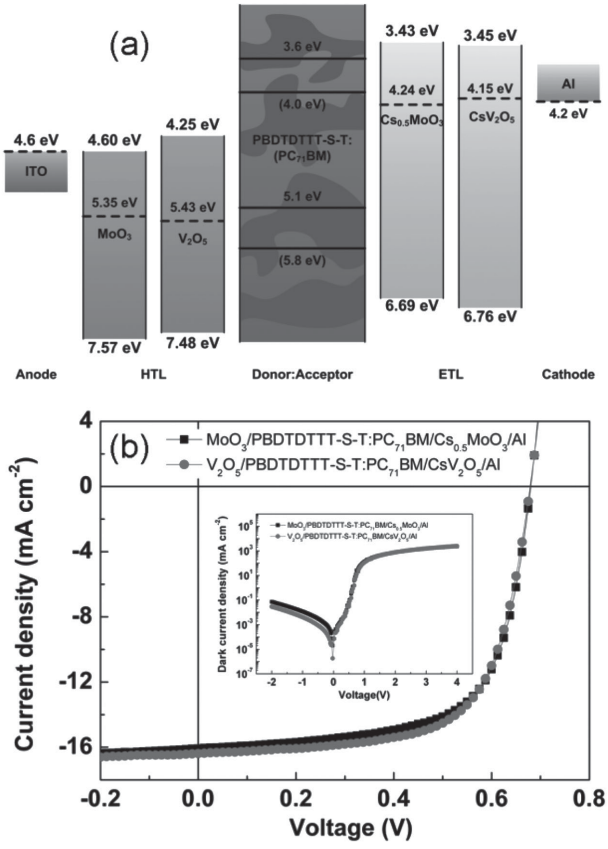

Figure 3. a) The schematic energy level diagrams of OSCs with structures of ITO/MoO_3/PBDTDTTT-S-T:$PC_{71}BM$/$Cs_{0.5}MoO_3$/Al and ITO/V_2O_5/PBDTDTTT-S-T:$PC_{71}BM$/CsV_2O_5/Al. b) Current density–voltage (*J–V*) characteristics of OSCs using different metal oxides as carrier transport layers. (Inset: Dark current density–voltage (J_{dark}–*V*) characteristics of OSCs with different structures.)

theoretical analysis of the generalized Shockley equation of *J–V* characteristics and the FF by photovoltaic effect indicates the strong limitation by the series and shunt resistance in solar cells,[21] which also explain that the non-Ohmic contact causes the carriers accumulation at the interface and the energy loss of the carriers to overcome the potential barrier.[15] As shown in Figure 5d, it is also found that the PCE has the nearly quadratic relationship with ΔE_F when the potential difference keeps decreasing. In other words, when there is potential barrier formed at the interface, a small decrease of ΔE_F will cause a larger drop of PCE of the device with regard to the device parameters of V_{OC}, J_{SC}, and FF.

2.2.2. OLEDs with Cs Intercalated Metal Oxides as both ETL and HTL

In this study, OLEDs are fabricated with the normal structures of ITO/MoO_3(8 nm)/P-PPV/$Cs_{0.5}MoO_3$(10 nm)/Al(100 nm) and ITO/V_2O_5(8 nm)/P-PPV/CsV_2O_5(10 nm)/Al(100 nm). Cs intercalated MoO_3 and V_2O_5 and pristine metal oxides have been demonstrated in OLEDs as both of ETLs and HTLs. The solution-processed light emitting layer is spin-coated with the thickness of 80 nm onto HTLs of MoO_3 and V_2O_5 by using the poly[2-(4-(3',7'-dimethyloctyloxy)-phenyl)-*p*-phenylene-vinylene] (P-PPV).[22] A conventional OLED with non-metal oxides structure of ITO/PEDOT:PSS/P-PPV/LiF/Al is also fabricated for comparison purpose. Details of OLEDs fabrication methods can be found in the experimental section.

Figure 6a,b shows the current density–voltage–luminance (*J–V–L*) and luminance efficiency–current density–luminance (LE–*J–L*) characteristics of OLEDs with different devices structures. OLED with MoO_3 based carrier transport layers gives a turn-on voltage at 5.25 V and a maximum luminance 23 300 cd m^{-2} at 11.75 V. Meanwhile, OLED with V_2O_5 based carrier transport layers shows a turn-on voltage at 5.00 V and the maximum luminance 31 000 cd m^{-2} at 11.25 V. Devices using metal oxides demonstrate obvious enhancement compared to the control OLED with a turn-on voltage at 6 V and a maximum luminance 23 155 cd m^{-2} at 13.75 V. The corresponding normalized electroluminescent spectra of different structure OLEDs are shown in Figure S5 in Supporting Information. The air stabilities test of un-encapsulated OLEDs with different HTLs and ETLs are given in Figure S6 in Supporting Information. OLEDs with metal oxides as carrier transport layers have much steeper *J–V* characteristics, which reveal better conductivity compared to the control device. Even though the current efficient of the control OLED is better at the low emission intensity, the current efficient of the metal oxide based OLEDs are similar to (in some case even better than) that of the control OLEDs when emission intensity is bigger than 500 Cd m^{-2}. Inverted OLEDs with metal oxides as HTL and ETL can also be fabricated with the structures of ITO/$Cs_{0.5}MoO_3$/P-PPV/MoO_3/Ag and ITO/CsV_2O_5/P-PPV/V_2O_5/Ag. The inverted device with MoO_3 based carrier transport layers gives a turn-on voltage at 5.25 V and a maximum luminance 22 383 cd m^{-2} at 11.75 V. And the inverted device with V_2O_5 based carrier transport layers shows a turn-on voltage at 4.75 V and the maximum luminance 28 516 cd m^{-2} at 11.5 V. Consequently, the larger luminance and lower turn-on voltage indicate metal oxides offer more efficient charge injection. Besides, the smoother roll-off luminance efficiency of the metal oxides based OLEDs reflects that the metal oxides have very good energy level alignment ability with adjacent organic layers at different electric fields.

Table 2. Device parameters of optimized OSCs using different metal oxides as carrier transport layers. The series resistance (R_S) of each device is calculated from the slope of the dark current density–voltage (J_{dark}–V) curves at a forward biased voltage of 2 V.

OSCs structures	V_{OC} (V)	J_{SC} [mA cm^{-2}]	FF [%]	PCE [%]	R_S [Ω cm^2]
MoO_3/$Cs_{0.5}MoO_3$	0.68 ± 0.006	16.08 ± 0.576	66.94 ± 0.836	7.32 ± 0.190	1.41 ± 0.127
V_2O_5/CsV_2O_5	0.68 ± 0.005	16.38 ± 0.460	67.23 ± 1.572	7.49 ± 0.156	1.29 ± 0.157

3. Conclusion

In summary, we have demonstrated over 1.1 eV workfunction tuning of metal oxides including MoO_3 and V_2O_5 by using Cs intercalation. The synthesized Cs intercalated metal oxides have the interesting features

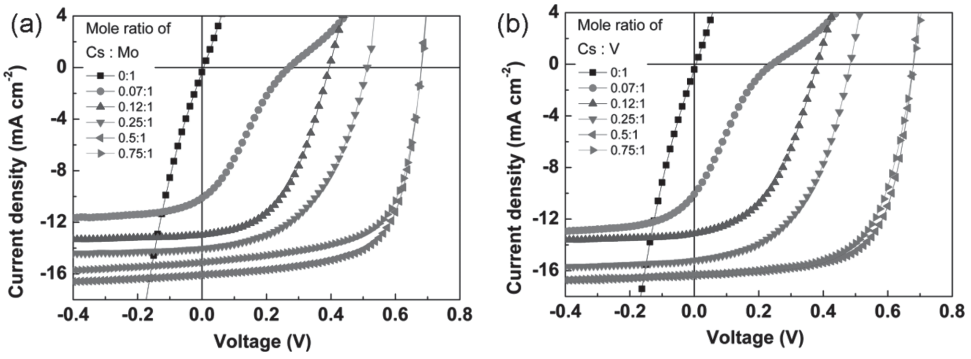

Figure 4. *J–V* characteristics of OSCs using Cs intercalated metal oxides as ETLs with different Cs ratio. a) OSCs with MoO_3 as HTL and Cs_xMoO_3 as ETL; b) OSCs with V_2O_5 as HTL and $Cs_xV_2O_5$ as ETL.

of room temperature and pressures, water free and solution process. We have also investigated the band structures and electrical properties of the Cs intercalated metal oxides for understanding the large workfunction tuning abilities. The results show that by using Cs intercalation, each of the metal oxides can function as both ETL and HTL in OSCs and OLEDs. The metal oxides based OSCs show compatible performances to that of the typical PEDOT:PSS based OSCs. In addition, OLEDs with Cs intercalated metal oxides as carrier transport layers has clear improvement the charge injection compared to the traditional non-metal oxide device made from PEDOT:PSS/LiF as HTL and ETL. Consequently, this new approach of Cs intercalated metal oxides with large workfunction tuning abilities can contribute to the evolution of applying metal oxides in high performance organic optoelectronic devices.

4. Experimental Section

Synthesis of Cesium Intercalated Metal Oxides: Molybdenum powder, vanadium powder and cesium carbonate powder were purchased from Aladdin Industrial Inc. The Cs intercalated metal oxides films were formed from cesium molybdenum bronze solution and cesium vanadium bronze solution. The solutions were obtained by blending the metal bronze solutions with Cs_2CO_3 solution at different calculated mole ratio and finally diluted with ethanol to have an optimized Cs intercalated metal oxides thickness after spin-coating. To obtain cesium molybdenum bronze solution and cesium vanadium bronze solution, the Cs_2CO_3 powder was firstly dissolved into 2-methoxyethanol at a high concentration of 10 mg mL^{-1}. 0.1 g molybdenum metal powder and 0.1 g vanadium metal powder was dispersed into 10 mL ethanol with ultrasonic bath. 0.3 ml hydrogen peroxide (30%) was added into molybdenum ethanol solution and 0.5 ml hydrogen peroxide was added into vanadium ethanol solution respectively. After 24 hours reaction with magnetic stirrer, the remaining solvents were vaporized in a dry box and followed by dissolving into ethanol with a concentration of 1 mg mL^{-1}. The Cs_2CO_3 solution was dropwise added into metal bronze solutions with a calculated volume ratio. The final Cs metal bronze solutions were diluted with ethanol to 1 mg mL^{-1} of the total concentration. Further details of the synthesis can be found in Supporting Information.

Fabrication of OSCs Devices: The OSCs with structures of ITO/MoO_3/PBDTDTTT-S-T:$PC_{71}BM$/Cs_xMoO_3/Al and ITO/V_2O_5/PBDTDTTT-S-T:$PC_{71}BM$/$Cs_xV_2O_5$/Al respectively were fabricated by the following procedures. The ITO/glass substrate was cleaned with detergent, acetone, ethanol, and UV-ozone treatment for each of 15 min. The sheet resistance of the ITO/glass was 15 Ω $Å^{-1}$. The MoO_3 and V_2O_5 films were formed by spin-coating molybdenum and vanadium bronze solution at 3000 rpm for 30 s onto the cleaned ITO substrates. The films thickness of MoO_3 and V_2O_5 are 8 nm which were measured

Table 3. Summary of device parameters of OSCs using Cs intercalated metal oxides with different Cs ratio as carrier transport layers.

Mole ratio of Cs : Mo or V		ΔE_F [eV]	V_{OC} [mV]	J_{SC} [mA cm^{-2}]	FF [%]	PCE [%]
MoO_3/Cs_xMoO_3	0 : 1	0	0	0	0	0
	0.07 : 1	0.29	275	10.12	26.16	0.73
	0.12 : 1	0.48	400	12.98	47.64	2.47
	0.25 : 1	0.79	512	14.04	49.26	3.55
	0.5 : 1	1.04	680	16.08	66.94	7.32
	0.75 : 1	1.15	680	15.12	65.18	6.70
V_2O_5/$Cs_xV_2O_5$	0 : 1	0	0	0	0	0
	0.07 : 1	0.26	237	10.07	22.17	0.53
	0.12 : 1	0.50	375	13.12	46.48	2.28
	0.25 : 1	0.84	475	15.21	48.71	3.28
	0.5 : 1	1.22	680	16.38	67.23	7.49
	0.75 : 1	1.29	680	16.28	63.37	7.02

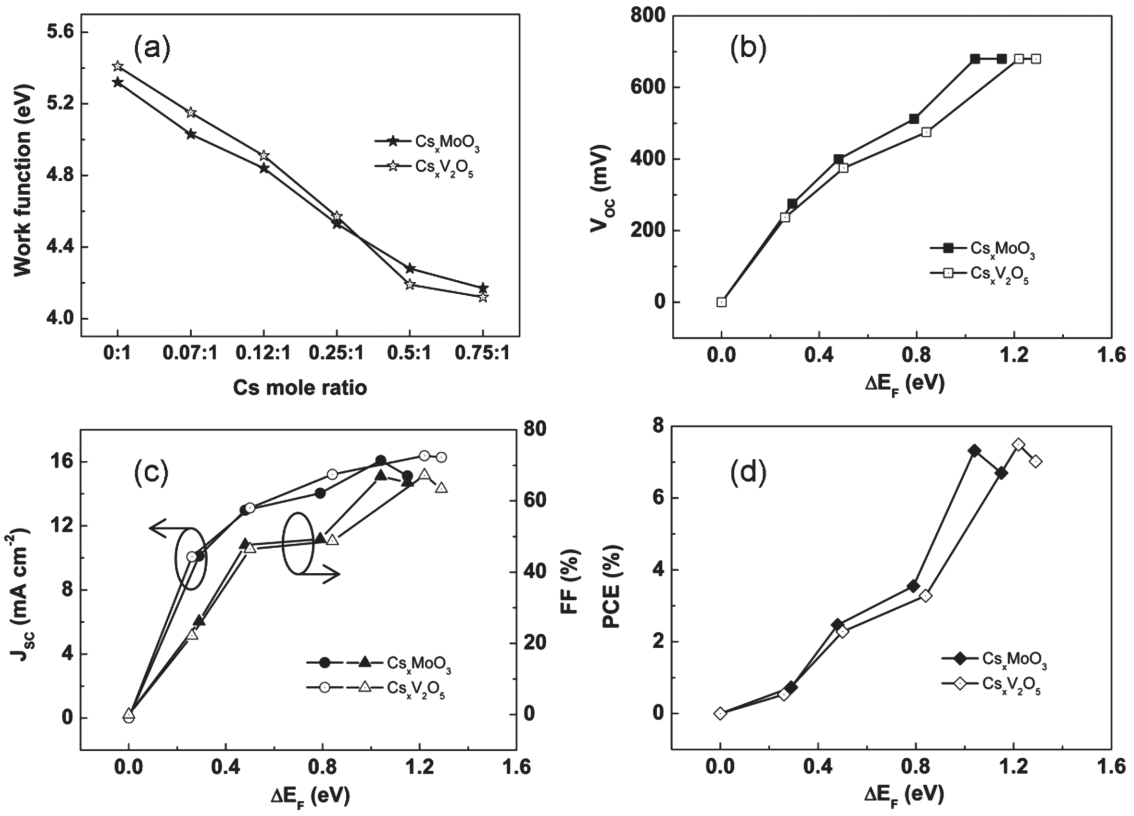

Figure 5. a) The workfunction variation of Cs intercalated metal oxides with different Cs ratio. b–d) The dependence of OSCs parameters on the energy-level offset (ΔE_F) between the HTL and the ETL, in details of b) open-circuit voltage (V_{OC}), c) short-circuit current density (J_{SC}) and fill factor (FF), d) power conversion efficiency (PCE).

by ellipsometry. The blended solution of PBDTDTTT-S-T:$PC_{71}BM$ was prepared in chlorobenzene (CB) at the concentration of 8 mg mL^{-1}:12 mg mL^{-1} with addition 3% v/v 1,8-diiodooctane (DIO). After the HTL formation, the blended solution was spin-coated onto the substrate at 2500 rpm for 50 s with a thickness of 110 nm, followed by 10 Pa vacuum treatment for 3 h to remove DIO. Cs_xMoO_3 and $Cs_xV_2O_5$ films were formed by spin-coating prepared solution directly onto the active layers at 3000 rpm for 40 s with a thickness of 10 nm. The top electrode of Al of a thickness 100 nm was finally thermally evaporated onto the top interfacial layers with a shadow mask of 0.06 cm^2 area.

Fabrication of OLEDs Devices: Active material of P-PPV solution was firstly prepared in p-Xylene at a concentration of 8 mg mL^{-1}. The OLEDs with structures of ITO/MoO_3/P-PPV/Cs_xMoO_3/Al and ITO/V_2O_5/P-PPV/$Cs_xV_2O_5$/Al were fabricated by the following procedures. HTLs of MoO_3 and V_2O_5 films were spin-coated onto the pre-cleaned ITO substrates with the same procedures as OSCs. The active layer was formed by spin-coated the P-PPV solution at 2000 rpm for 60 s with a thickness of 80 nm. ETLs of Cs intercalated MoO_3 and V_2O_5 were fabricated using the same procedure as OSCs. For conventional structure OLEDs of ITO/PEDOT:PSS/P-PPV/LiF/Al, PEDOT:PSS was firstly spin-coated onto ITO substrate at 3000 rpm for 40 s with a thickness of 40 nm, followed by thermally baking process at 120 °C for 20 min. After the active layer formation, ETL of LiF was evaporated in a vacuum chamber of 1 nm. Finally, the top electrode of Al of a thickness 100 nm was thermally evaporated onto the ETLs with a shadow mask of 0.06 cm^2 area. The inverted structure OSCs and OLEDs were fabricated with thermally evaporated 100 nm Ag onto the HTL metal oxides with a shadow mask of 0.06 cm^2 area.

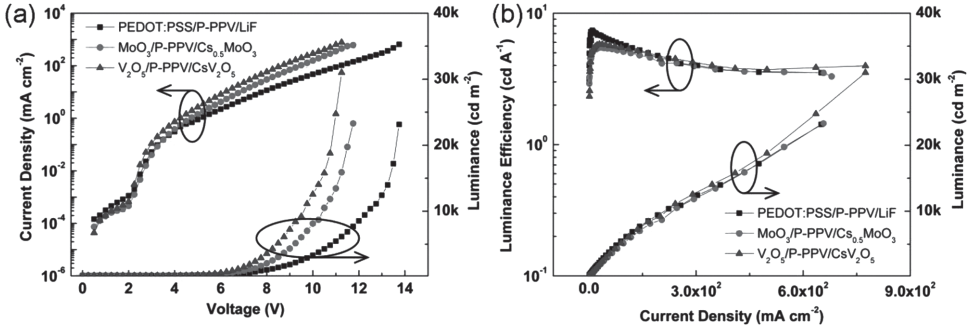

Figure 6. Respective a) current density–voltage–luminance (*J*–*V*–*L*) and luminance efficiency–current density–luminance (LE–*J*–*L*) characteristics of OLEDs with different carrier transport layers.

Measurement and Characterization: The current density–voltage (*J–V*) characterizations of the OSCs were measured by using a Keithley 2635 source meter and an ABET AM 1.5 G solar simulator with a light intensity of 100 mW cm^{-2}. The series resistance (R_S) of each device is calculated from the slope of the dark current density-voltage (J_{dark}–V) curves at a forward biased voltage of 2 V. The statistical errors of each parameter are sampled at least of 10 devices. The current density-voltage-luminance (*J–V–L*) and luminance efficiency-current density-luminance (LE–*J–L*) characteristics of OLEDs were measured by using a Keithley 2635 source meter and a calibrated Si photodiode. Normalized electroluminance spectra were recorded by an Oriel spectrometer with a charge-coupled device detector. The thickness and the optical band gap of different carrier transport layers were measured by spectroscopic ellipsometry (J.A. WOOLLAM CO. INC.). The workfunction of different carrier transport layers were measured by a SKP5050 Scanning Kelvin Probe System (KP Technology Ltd.) with a resolution 1–3 meV. The results of Kelvin probe force microscope (KPFM) was measured by using MultiMode 8 of Bruker Corporation. UPS measurement was taken by He I discharge lamp (Kratos Analytical) with energy of 21.22 eV and a resolution of 0.15 eV. A –10 V bias was added to enhance the measured signals on the samples. EDX results and elements analysis are measured by FEI Tecnai G2 20 S-TWIN Scanning Transmission Electron Microscope.

Supporting Information

Supporting Information is available from the Wiley Online Library or from the author.

Acknowledgements

This work is supported by University Grant Council of the University of Hong Kong (grants #10401466), and the General Research Fund (grants: HKU711813 and HKU711612E), the RGC-NSFC grant (N_HKU709/12) from the Research Grants Council of Hong Kong Special Administrative Region, China and the research fund (M-HKU703/12) from the Specialized Research Fund for the Doctoral Program of Higher Education (SRFDP) and Research Grants Council Earmarked Research Grants (RGC ERG) Joint Research Scheme. Jianhui Hou would like to thank the financial support by NSFC (No. 51261160496) and Chinese Academy of Sciences (KJZD-EW-J01).

Received: June 16, 2014
Revised: July 26, 2014
Published online: September 11, 2014

[1] V. D. Mihailetchi, L. J. A. Koster, J. C. Hummelen, P. W. M. Blom, *Phys. Rev. Lett.* **2004**, *93*, 216601.

[2] a) L. J. A. Koster, E. C. P. Smits, V. D. Mihailetchi, P. W. M. Blom, *Phys. Rev. B* **2005**, *72*, 085205; b) G. Li, Y. Yao, H. Yang, V. Shrotriya, G. Yang, Y. Yang, *Adv. Funct. Mater.* **2007**, *17*, 1636; c) C. W. Tang, S. A. VanSlyke, *Appl. Phys. Lett.* **1987**, *51*, 913; d) S. Reineke, F. Lindner, G. Schwartz, N. Seidler, K. Walzer, B. Lussem, K. Leo, *Nature* **2009**, *459*, 234; e) W.-Y. Wong, X.-Z. Wang, Z. He, A. B. Djurisic, C.-T. Yip, K.-Y. Cheung, H. Wang, C. S. K. Mak, W.-K. Chan, *Nat. Mater.* **2007**, *6*, 521; f) J. You, L. Dou, K. Yoshimura, T. Kato, K. Ohya, T. Moriarty, K. Emery, C.-C. Chen, J. Gao, G. Li, Y. Yang, *Nat. Commun.* **2013**, *4*, 1446; g) Y. He, H.-Y. Chen, J. Hou, Y. Li, *J. Am. Chem. Soc.* **2010**, *132*, 1377; h) Y. Liang, Z. Xu, J. Xia, S.-T. Tsai, Y. Wu, G. Li, C. Ray, L. Yu, *Adv. Mater.* **2010**, *22*, E135; i) G. Li, R. Zhu, Y. Yang, *Nat. Photonics* **2012**, *6*, 153; j) Y. Dong, X. Hu, C. Duan, P. Liu, S. Liu, L. Lan, D. Chen, L. Ying, S. Su, X. Gong, F. Huang, Y. Cao, *Adv. Mater.* **2013**, *25*, 3683; k) A. Rao, P. C. Y. Chow, S. Gelinas, C. W. Schlenker, C.-Z. Li, H.-L. Yip, A. K. Y. Jen, D. S. Ginger, R. H. Friend, *Nature* **2013**, *500*, 435; k) H. Ma, H.-L. Yip, F. Huang, A. K. Y. Jen, *Adv. Funct. Mater.* **2010**, *20*, 1371; l) Z. He, C. Zhong, S. Su, M. Xu, H. Wu, Y. Cao, *Nat. Photonics* **2012**, *6*, 591; m) F. Huang, H. Wu, Y. Cao, *Chem. Soc. Rev.* **2010**, *39*, 2500; n) Y.-J. Cheng, C.-H. Hsieh, Y. He, C.-S. Hsu, Y. Li, *J Am Chem Soc* **2010**, *132*, 17381; o) H. Zheng, Y. Zheng, N. Liu, N. Ai, Q. Wang, S. Wu, J. Zhou, D. Hu, S. Yu, S. Han, W. Xu, C. Luo, Y. Meng, Z. Jiang, Y. Chen, D. Li, F. Huang, J. Wang, J. Peng, Y. Cao, *Nat Commun* **2013**, *4*; p) Q. Zhang, B. Li, S. Huang, H. Nomura, H. Tanaka, C. Adachi, *Nat. Photonics* **2014**, *8*, 326.

[3] F. Xie, W. C. H. Choy, C. Wang, X. Li, S. Zhang, J. Hou, *Adv. Mater.* **2013**, *25*, 2051.

[4] a) Y. Cao, G. Yu, I. D. Parker, A. J. Heeger, *J. Appl. Phys.* **2000**, *88*, 3618; b) H. Kim, C. M. Gilmore, J. S. Horwitz, A. Piqué, H. Murata, G. P. Kushto, R. Schlaf, Z. H. Kafafi, D. B. Chrisey, *Appl. Phys. Lett.* **2000**, *76*, 259.

[5] a) C. Girotto, E. Voroshazi, D. Cheyns, P. Heremans, B. P. Rand, *ACS Appl. Mater. Interfaces* **2011**, *3*, 3244; b) J. J. Jasieniak, J. Seifter, J. Jo, T. Mates, A. J. Heeger, *Adv. Funct. Mater.* **2012**, *22*, 2594; c) J. R. Manders, S.-W. Tsang, M. J. Hartel, T.-H. Lai, S. Chen, C. M. Amb, J. R. Reynolds, F. So, *Adv. Funct. Mater.* **2013**, *23*, 2993; d) S. Murase, Y. Yang, *Adv. Mater.* **2012**, *24*, 2459; e) J. Y. Kim, S. H. Kim, H. H. Lee, K. Lee, W. Ma, X. Gong, A. J. Heeger, *Adv. Mater.* **2006**, *18*, 572.

[6] a) C. H. Bamford, C. F. H. Tipper, *Degradation of polymers*, Vol. *14*, Elsevier Science Ltd, Amsterdam **1975**; b) K. Kawano, C. Adachi, *Adv. Funct. Mater.* **2009**, *19*, 3934.

[7] M. T. Greiner, M. G. Helander, W. M. Tang, Z. B. Wang, J. Qiu, Z. H. Lu, *Nat. Mater.* **2011**, *11*, 76.

[8] V. Shrotriya, G. Li, Y. Yao, C.-W. Chu, Y. Yang, *Appl. Phys. Lett.* **2006**, *88*, 073508.

[9] G. Li, C.-W. Chu, V. Shrotriya, J. Huang, Y. Yang, *Appl. Phys. Lett.* **2006**, *88*, 253503.

[10] X. Li, W. C. H. Choy, F. Xie, S. Zhang, J. Hou, *J. Mater. Chem. A* **2013**, *1*, 6614.

[11] X. W. Lou, H. C. Zeng, *Chem. Mater.* **2002**, *14*, 4781.

[12] a) J. Yang, F. Lu, Y. Li, S. Yang, R. Li, N. Huo, C. Fan, Z. Wei, J. Li, S.-S. Li, *J. Mater. Chem. C* **2014**, *2*, 1034; b) C. Li, R. Xiong, D. Yin, Z. Tang, J. Wang, D. Li, Z. Yu, J. Shi, *J. Cryst. Growth* **2005**, *285*, 81; c) J. Lu, C. Sun, M. Zheng, Y. Wang, M. Nripan, J. A. van Kan, S. G. Mhaisalkar, C. H. Sow, *J. Phys. Chem. C* **2012**, *116*, 22015; d) J. Liu, S. Shao, G. Fang, B. Meng, Z. Xie, L. Wang, *Adv. Mater.* **2012**, *24*, 2774; e) D. M. Yu, S. T. Zhang, D. W. Liu, X. Y. Zhou, S. H. Xie, Q. F. Zhang, Y. Y. Liu, G. Z. Cao, *J. Mater. Chem.* **2010**, *20*, 10841; f) H. Yu, X. Rui, H. Tan, J. Chen, X. Huang, C. Xu, W. Liu, D. Y. W. Yu, H. H. Hng, H. E. Hoster, Q. Yan, *Nanoscale* **2013**, *5*, 4937; g) Y. Li, J. Yao, E. Uchaker, M. Zhang, J. Tian, X. Liu, G. Cao, *J. Phys. Chem. C* **2013**, *117*, 23507.

[13] H.-H. Liao, L.-M. Chen, Z. Xu, G. Li, Y. Yang, *Appl. Phys. Lett.* **2008**, *92*, 173303.

[14] a) M.-H. Park, J.-H. Li, A. Kumar, G. Li, Y. Yang, *Adv. Funct. Mater.* **2009**, *19*, 1241; b) J. You, C.-C. Chen, L. Dou, S. Murase, H.-S. Duan, S. A. Hawks, T. Xu, H. J. Son, L. Yu, G. Li, Y. Yang, *Adv. Mater.* **2012**, *24*, 5267.

[15] V. D. Mihailetchi, P. W. M. Blom, J. C. Hummelen, M. T. Rispens, *J. Appl. Phys.* **2003**, *94*, 6849.

[16] a) J. G. Lu, S. Fujita, T. Kawaharamura, H. Nishinaka, Y. Kamada, T. Ohshima, Z. Z. Ye, Y. J. Zeng, Y. Z. Zhang, L. P. Zhu, H. P. He, B. H. Zhao, *J. Appl. Phys.* **2007**, *101*, 083705; b) E. Burstein, *Phys. Rev.* **1954**, *93*, 632; c) T. Moss, *Proc. Phys. Soc. B* **1954**, *67*, 775.

[17] Y. Huang, X. Guo, F. Liu, L. Huo, Y. Chen, T. P. Russell, C. C. Han, Y. Li, J. Hou, *Adv. Mater.* **2012**, *24*, 3383.

[18] K. Walzer, B. Maennig, M. Pfeiffer, K. Leo, *Chem. Rev.* **2007**, *107*, 1233.
[19] P. Schilinsky, C. Waldauf, J. Hauch, C. J. Brabec, *J. Appl. Phys.* **2004**, *95*, 2816.
[20] a) M. C. Scharber, D. Mühlbacher, M. Koppe, P. Denk, C. Waldauf, A. J. Heeger, C. J. Brabec, *Adv. Mater.* **2006**, *18*, 789; b) C. J. Brabec, A. Cravino, D. Meissner, N. S. Sariciftci, T. Fromherz, M. T. Rispens, L. Sanchez, J. C. Hummelen, *Adv. Funct. Mater.* **2001**, *11*, 374; c) A. Gadisa, M. Svensson, M. R. Andersson, O. Inganäs, *Appl. Phys. Lett.* **2004**, *84*, 1609.
[21] J. D. Servaites, S. Yeganeh, T. J. Marks, M. A. Ratner, *Adv. Funct. Mater.* **2010**, *20*, 97.
[22] H. Becker, H. Spreitzer, W. Kreuder, E. Kluge, H. Schenk, I. Parker, Y. Cao, *Adv. Mater.* **2000**, *12*, 42.